Noise Parameters of CW Radar Sensors Used in Active Defense Systems

Vojtech JENIK [1], Premysl HUDEC [1], Petr PANEK [2]

[1] Dept. of Electromagnetic Field, Czech Technical University in Prague, Technicka 2, 160 00 Prague 6, Czech Republic
[2] Inst. of Photonics and Electronics, Academy of Science of the Czech Rep., Chaberska 57, 182 51 Praha 8, Czech Rep.

jenikvoj@fel.cvut.cz, hudecp@fel.cvut.cz, p.panek@volny.cz

Abstract. *Active defense represents an innovative way of protecting military vehicles. It is based on the employment of a set of radar sensors which detect an approaching threat missile and activate a suitable counter-measure. Since the radar sensors are supposed to detect flying missiles very fast and, at the same time, distinguish them from stationary or slow-moving objects, CW Doppler radar sensors can be employed with a benefit. The submitted article deals with a complex noise analysis of this type of sensors. The analysis considers the noise of linear and quasi-linear RF components, phase-noise of the local oscillator as well as the noise of low-frequency circuits. Since the incidence of the phase-noise depends strongly upon the time delay between the reference and the cross-talked signals, a new method of measuring noise parameters utilizing a reflecting wall has been developed and verified. The achieved results confirm potentially high influence of the phase-noise on the noise parameters of the mentioned type of radar sensors. Obtained results can be used for the analysis of noise parameters of the similar but even more complex sensors.*

Keywords

CW radar sensor, noise parameters, noise measurement, active defense.

1. Introduction

In general, the CW radars are considered to be comparatively simple types of radars with a limited detection range and capabilities. On the other hand, they have many advantages. Not only are they relatively simple, small and low-cost, but they also offer a zero blind-zone and ability to detect reliably moving objects. Thus their application in different systems can be very beneficial. Descriptions of CW radar sensors designed for automotive applications can be found e. g. in [1] and [2]. Similar sensors are often used for monitoring vital signs in medicine applications, examples are presented in [3], [4] and [5]. In [5], a short noise analysis can also be found. Paper [6] describes the utilization of a Doppler CW radar sensor for flow measurements.

Since the CW radar sensors are able to measure even very fast moving objects, they can be used with a benefit for the detection of missiles in military applications. The descriptions of CW radar sensors capable of detecting the approaching missiles have been published e.g. in [7] - [9]. In this application, the subjective CW sensors form the parts of active defense (AD) systems. They represent a new way how to solve problems with the protection of military vehicles against various types of threat missiles. Some of the most dangerous ones are described in [7]. Nowadays, big attention is especially paid to hand-held cumulative missiles (e. g. RPG-7). In spite of being relatively simple and low-cost, their efficiency is so high that they are able to penetrate up to 300 mm of the best steel armors and destroy nearly any military vehicle. Millions of these cumulative missiles are deployed in the most dangerous hot spots in third-world countries and represent one of the greatest threats in the fight against terrorism. Therefore, intensive research efforts are aimed at the development of efficient and reliable protection.

Fig. 1. Test CW radar sensor during practical tests at army shooting range.

The AD systems are based on the radar sensors able to detect approaching threat missiles and activate suitable counter-measure. It should be capable of destroying or deactivating the attacking missile. The radar sensors used in the above referred AD systems must be able to detect the threat missiles even in a close proximity of the protected vehicles. In addition, they have to distinguish the fast

moving targets (100 – 1700 m/s) from all stationary or slow-moving objects. As a result, the CW radar sensors with a zero blind-zone and direct Doppler processing can be a very good option. Fig. 1 shows the sample of the CW radar sensor operated at 11 GHz, equipped with two patch antennas in practical tests in an army shooting range. The monitored RPG-7 missiles flew just under the sensor.

Fig. 2 demonstrates the spectrogram calculated from the data recorded in one of the tests. At a time of 0.1 s, the missile was shot out from a stand launcher. After 20 ms, the rocket motor was activated and the velocity of the missile started to rise. After following 130 ms, the missile flew directly under the sensor and the measured Doppler frequency dropped to zero. The Doppler frequency at the beginning of the flight is about 9 kHz, which corresponds to the initial flight velocity of the missile equal to 123 m/s. The measured maximum Doppler frequency is 12 kHz, which corresponds to the missile's velocity of 164 m/s. All measured parameters correspond proficiently to the expected behavior of the RPG-7 missile.
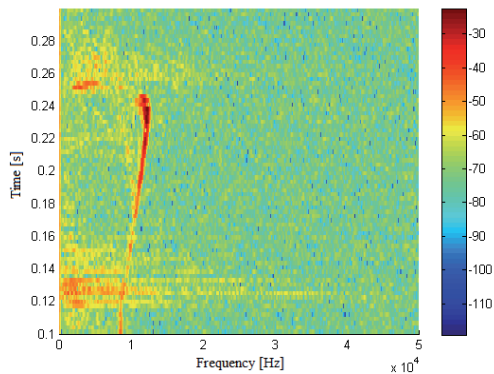

Fig. 2. Spectrogram of flight of RPG-7 missile.

The above-presented results show that the CW radar sensors are able to monitor the missile both in a medium range and in a close proximity of the protected vehicle. Moreover, they provide the data important for the activation of the counter-measures. Additional information about the used signal-processing methods can be found in [9]. As many important parameters of the CW radar sensors and signal-processing procedures depend substantially on signal-to-noise and signal-to-interferences ratios, detailed noise analyses and measurements are, therefore, crucial.

2. CW Radar Sensors

There is a variety of different CW radar structures ranging from relatively simple to more complex, including IF processing and different forms of modulation, which also enable measuring the distance of the monitored targets. All the structures in question are derived from a basic circuit based on a coherent mixing. This circuit was also employed in the first AD system tests and described in the presented noise analysis. The subsequent work revealed that the noise analyses of more complex CW radar sensors

lead to very similar or even identical results. This concerns, for example, the frequency-hopping radar or BPSK pseudo-noise radar, both still under the development.
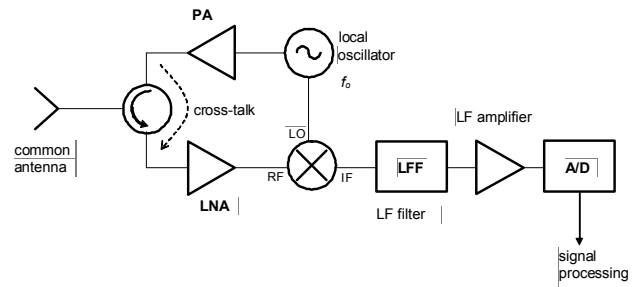

Fig. 3. Basic CW radar structure with common antenna.

Fig. 3 shows a fundamental CW radar structure, where the transmitter and receiver share the same antenna that is coupled by a circulator. The transmitted wave is generated by a local oscillator and amplified by the power amplifier (PA). In our case, for the construction of the oscillators, the dielectric resonator oscillator (DRO) or PLL based circuits are used. The received signal reflected from the target is amplified by a low-noise amplifier (LNA) and coherently mixed with the reference signal. The subsequent filter selects the output low-frequency (LF) signals and rejects all other signals. In case of moving targets, the coherent mixing provides an LF signal with a frequency equal to the Doppler shift between the transmitted and received signals. The DC component generated by the reflections from stationary objects is easily removable by means of an LF filter. Beside the signal reflected from the target, it is indispensable to consider the cross-talked signal caused by either a limited isolation of the circulator or by a reflection of the transmitted signal from the antenna. The cross-talked signal can give rise to the limitation of the LNA and, as it will be shown later in the text, it can influence the noise parameters of the radar sensor as well. Therefore, the structures with separate transmitting and receiving antennas are utilized frequently; see Fig. 4.
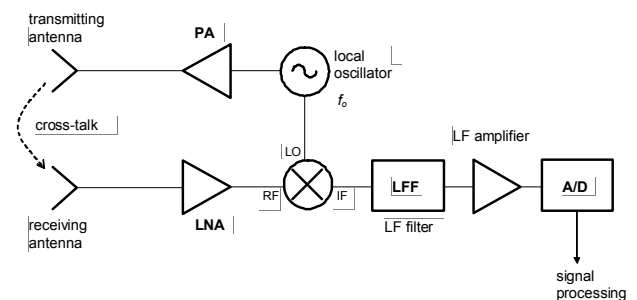

Fig. 4. Basic CW radar structure with separated antennas.

Due to the use of two spatially separated antennas, a lower cross-talk between the transmitter and receiver can be achieved. Yet in this case, the time-shift between the reference and cross-talked signals is longer and subject to considerable fluctuations. All radar sensors used during the practical measurements indicated below were based on the 'two-antenna' structure.

3. Noise Sources within CW Radar Sensors

Noise sources of the CW radar sensors can be divided into the following categories:

- Noise of linear or quasi-linear RF circuits of the receiver
- Phase-noise of the local oscillator
- Noise of the LF circuits

All the above-mentioned sources were analyzed separately and summed up at the LF filter output.

3.1 Noise of Linear or Quasi-Linear RF Receiver Circuits

The model of a CW radar receiver comprising the linear and quasi-linear RF circuits can be found in Fig. 5.
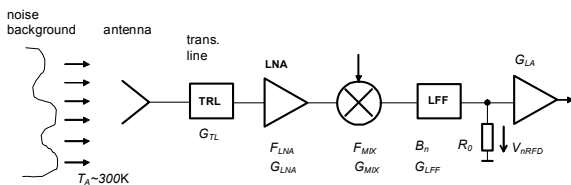

Fig. 5. Model of CW radar receiver including linear or quasi-linear RF circuits.

Apart from the passive circuits (antenna, transmission line, filter), the model involves an LNA, mixer and LF amplifier that can be treated as quasi-linear components here. In Fig. 5, T_A represents noise temperature of the noise background, typically, $T_A \sim 300$ K. That is why, in this case, the antenna can be modeled as a matched load with standard noise temperature T_0. Yet problems originating from the receiving antenna seeing the plasma of nearby explosions should not be omitted, for example, by using higher reserves in the system design. Since the antennas in the AD systems are frequently damaged or even destroyed by the activated counter-measure, they are, in order to protect the main parts of the sensors, connected using the sections of co-axial cables. Their influence can be described by the G_{TL} parameter.

The noise power P_{nRF} at the output of the receiver caused by either linear or quasi-linear RF circuits can be described by the formula (1):

$$P_{nRF} = kT_0 B_n G_{TL} G_{LNA} G_{MIX} G_{LFF} +$$
$$+ (1/G_{TL} - 1) B_n kT_0 G_{TL} G_{LNA} G_{MIX} G_{LFF} +$$
$$+ (F_{LNA} - 1) B_n kT_0 G_{LNA} G_{MIX} G_{LFF} +$$
$$+ (F_{MIX} - 1) B_n kT_0 G_{MIX} G_{LFF} +$$
$$+ (1/G_{LFF} - 1) B_n kT_0 G_{LFF}$$
(1)

In this formula, B_n describes the noise bandwidth, G_{LNA} and F_{LNA} represent the gain and noise figure of LNA respectively, while G_{MIX} and F_{MIX} stand for the conversion gain and noise figure of the mixer. In addition, G_{LFF} repre-

sents the gain of the passive LF filter. If a high-gain LNA is used, the P_{nRF} power is dominantly determined by first two items in (1) and the following items can be omitted. If a low-gain LNA or no LNA is utilized, influences of the mixer and LF filter can be significant and must be included into calculations. In case that the radar sensor does not reject the mirror frequencies, it is necessary to take into account the DSB noise power P_{nRFD}:

$$P_{nRFD} = 2P_{nRF} .$$
(2)

The effective value of the noise voltage V_{nRF} at the output of the LF filter loaded with the R_0 load and caused by the linear or quasi-linear RF components can be expressed as:

$$V_{nRF} = \sqrt{P_{nRFD} R_0} .$$
(3)

3.2 Phase-Noise of Local Oscillator

In order to calculate the influence of the phase-noise of the local oscillator, the entire transmitting – receiving chain has to be considered. The transmitted signal $s_t(t)$ can be described as:

$$s_t(t) = A_t \cos(2\pi f_o t + \Psi + \varphi(t)).$$
(4)

In this formula, A_t describes the signal voltage amplitude, f_o stands for the local oscillator frequency, Ψ represents the initial phase and $\varphi(t)$ is the phase-noise of the local oscillator. The phase-noise is a random process with power spectral density $S_\varphi(f)$. One part of the transmitted signal is used as a reference signal $s_r(t)$ and is brought to the LO input of the mixer.

$$s_r(t) = A_r \cos(2\pi f_o t + \Psi + \varphi(t)).$$
(5)

As it has already been mentioned, apart from the signal caused by the reflection from the target, there is always a cross-talked signal $s_{ct}(t)$ at the input of the mixer.

$$s_{ct}(t) = A_{ct} \cos(2\pi f_o(t-\tau) + \Psi + \varphi(t-\tau)).$$
(6)

The cross-talked signal with a voltage amplitude A_{ct} is an attenuated copy of the transmitted signal delayed by τ (with respect to the reference signal). In order to simplify the following formulae, all the above-defined signals share the same initial phase Ψ. The mixer converting the RF signal directly into the base-band can be described as a multiplier and its voltage conversion constant can be, together with the amplitude of the reference signal, included into the conversion gain G_{MIX}. The signal at the output of the mixer can be expressed as follows:

$$s_{MIX}(t) = \sqrt{G_{MIX}} A_{ct} \cdot$$
$$\cdot [\cos(4\pi f_o t - 2\pi f_o \tau + 2\Psi + \varphi(t) + \varphi(t-\tau)) +$$
$$+ \cos(2\pi f_o \tau + \varphi(t) - \varphi(t-\tau))]$$
(7)

The low-frequency filter LFF connected to the output of the mixer includes a low-pass section that suppresses all high-frequency components. A resulting low-frequency

(LF) signal $s_{LF}(t)$ can be described by the following formula:

$$s_{LF}(t) = \sqrt{G_{MIX}G_{LFF}}\, A_{ct} \cdot$$
$$\cdot \cos(2\pi f_o \tau + \Delta\varphi(t,\tau)) \qquad (8)$$

The signal contains only the DC component and noise, while $\Delta\varphi(t,\tau)$ represents the phase noise difference, described by formula (9). Supposing that the $\varphi(t)$ process can be linearized on the interval of the length τ, we can use an approximation:

$$\Delta\varphi(t,\tau) = \varphi(t) - \varphi(t-\tau) \approx \tau\frac{d\varphi(t)}{dt}. \qquad (9)$$

The formula (8) can be therefore rearranged into a form:

$$s_{LF}(t) = \sqrt{G_{MIX}G_{LFF}}\, A_{ct} \cdot$$
$$\cdot \cos(2\pi f_o \tau + \tau\frac{d\varphi(t)}{dt}) =$$
$$= \sqrt{G_{MIX}G_{LFF}}\, A_{ct}\left[\cos(2\pi f_o \tau)\cos(\tau\frac{d\varphi(t)}{dt}) - \right. \qquad (10)$$
$$\left. - \sin(2\pi f_o \tau)\sin(\tau\frac{d\varphi(t)}{dt})\right]$$

Supposing that $\Delta\varphi(t,\tau) \ll 1$, the linearization of the sine and cosine functions can be performed and the formula (10) reduced into a form:

$$s_{LF}(t) \cong \sqrt{G_{MIX}G_{LFF}}\, A_{ct} \cdot$$
$$\cdot\left[\cos(2\pi f_o \tau) - \tau\frac{d\varphi(t)}{dt}\sin(2\pi f_o \tau)\right] \qquad (11)$$

After removing a DC component by the high-pass filter which is also a part of the LFF, the power spectral density (PSD) of the LF noise caused by the phase-noise of the local oscillator $S_{nPN}(f)$ takes the form:

$$S_{nPN}(f) =$$
$$= G_{MIX}G_{LFF}\frac{A_{ct}^2}{R_0}\tau^2 \sin^2(2\pi f_o \tau)\, S_{\frac{d\varphi(t)}{dt}}(f) \qquad (12)$$

Supposing that there is a low frequency shift between the reference and cross-talked signals, e.g. due to the Doppler shift, it is possible to define the power of the cross-talked signal at the RF port of the mixer P_{ct}:

$$P_{ct} = \frac{A_{ct}^2}{2R_0} = P_{TX}G_{AA}G_{TL}G_{LNA}. \qquad (13)$$

G_{AA} in this formula represents a cross-talk gain, P_{TX} stands for a transmitted power and G_{LNA} is a low noise amplifier gain. Substituting (13) in (12), PSD of the objective signal can be expressed as:

$$S_{nPN}(f) = 2P_{TX}G_{MIX}G_{LFF}G_{AA}G_{TL}G_{LNA}\tau^2 \cdot$$
$$\cdot \sin^2(2\pi f_o \tau)\, S_{\frac{d\varphi(t)}{dt}}(f) \qquad (14)$$

In order to simplify the following formulae, it is possible to define the power P_{ctLF} of the cross-talked and frequency shifted signal at the output of the LF filter:

$$P_{ctLF} = P_{TX}G_{MIX}G_{LFF}G_{AA}G_{TL}G_{LNA}. \qquad (15)$$

Besides, PSD of the time derivation of the phase noise can be expressed as:

$$S_{\frac{d\varphi(t)}{dt}} = 4\pi^2 f^2 S_\varphi(f). \qquad (16)$$

Using formulae (15) and (16), the resulting value of $S_{nPN}(f)$ can be obtained.

$$S_{nPN}(f) =$$
$$= 8P_{ctLF}\pi^2\tau^2 f^2 \sin^2(2\pi f_o \tau)\, S_\varphi(f) \qquad (17)$$

The formula (17) shows that PSD is a strong function of the time delay τ between the reference and the cross-talked signals. For $\tau = 0$, this noise component equals zero. The higher the τ is, the higher the amplitude of oscillations of PSD between zero and local maxima $S_{nPNmax}(f)$, where:

$$S_{nPN\max}(f) = 8P_{ctLF}\pi^2\tau^2 f^2 S_\varphi(f) \qquad (18)$$

PSD of the oscillator phase noise can be approximated by the white phase and white frequency components using formula (19), which can be found e. g. in [11] or [12]:

$$S_\varphi(f) \approx a_0 + \frac{a_1}{f^2}. \qquad (19)$$

With the help of this phase-noise model, the resulting PSD can be expressed as:

$$S_{nPN}(f) =$$
$$= 8P_{ctLF}\pi^2\tau^2 \sin^2(2\pi f_o \tau)\left(a_0 f^2 + a_1\right) \qquad (20)$$

As it has been already mentioned, the LF filter consists of a high-pass filter with cut-off frequency f_{bl} and a low-pass filter with cut-off frequency f_{bh}. The high-pass filter removes reflections from the stationary or slow-moving objects, whereas the low-pass filter removes all frequencies above the highest expected Doppler frequency. Given the DSB conversion, the noise power P_{nPN} defined within the frequency band from f_{bl} to f_{bh} can be expressed as:

$$P_{nPN} =$$
$$= 16P_{ctLF}\pi^2\tau^2 \sin^2(2\pi f_o \tau)\int_{f_{bl}}^{f_{bh}}(a_0 f^2 + a_1)df \qquad (21)$$

Supposing $f_{bh} \gg f_{bl}$, the P_{nPN} noise power can be expressed as:

$$P_{nPN} \approx 16P_{ctLF}\pi^2\tau^2 \sin^2(2\pi f_o \tau)\left[\frac{a_0}{3}f_{bh}^3 + a_1 f_{bh}\right]. \qquad (22)$$

Subsequently, it is possible to express the resulting effective value of the noise voltage that arises from the phase-noise of the local oscillator V_{nPN} and is defined at the R_0 load.

$$V_{nPN} = \sqrt{P_{nPN}R_0} \; . \tag{23}$$

3.3 Noise of LF Circuits

Since the amplitudes of LF voltages at the output of the mixer (and also LF filter) can reach very low levels, it is necessary to connect a low-noise LF amplifier in front of A/D processing. Here it is advisable to employ a low-noise operational amplifier. In our case, LT1028 (Linear Technology) OA was used; see Fig. 6.
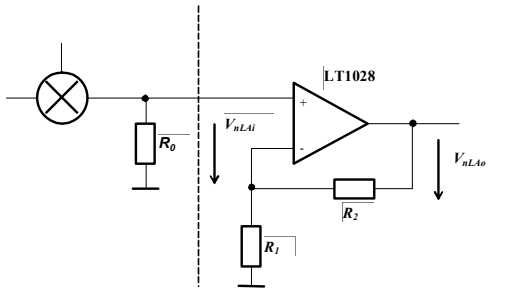

Fig. 6. Low-noise LF amplifier based on LT1028.

In case of the circuit in question, the manufacturer declares, see reference [10], that the effective value of the noise voltage V_{nLAi} referred to the input reaches the value:

$$V_{nLAi} = \sqrt{B_n \left[e_n^2 + e_{nR}^2 + (i_n R_{eq})^2 \right]} \; . \tag{24}$$

In this formula, e_n stands for the input noise voltage of the given OA (the value is stated in [nV.Hz$^{-1/2}$]) and i_n represents the input noise current of the given OA (the value is stated in [pA.Hz$^{-1/2}$]). The values of the noise voltages generated by the resistors can be calculated by formulae (25) and (26).

$$e_{nR} = \sqrt{4kT_0 R_{eq}} \; , \tag{25}$$

$$R_{eq} = R_0 / 2 + \frac{R_1 R_2}{R_1 + R_2} \; . \tag{26}$$

3.4 Resulting Noise Parameters

The resulting noise voltage V_{nri} can be defined as a RMS sum of all noise voltages at the R_0 load, connected at the input of the LF amplifier:

$$V_{nri} = \sqrt{V_{nRFD}^2 + V_{nLAi}^2 + V_{nPN}^2} \; . \tag{27}$$

Instead of more usual transformation of all noise sources to the receiver input, summing all noise components at the R_0 plane enables an easy interface of the RF and LF noise sources and leads to directly measurable values. The measurable noise voltage V_{nro} at the LF ampli-

fier output can be calculated by simple multiplying V_{nri} by a voltage gain A_L at the LF amplifier:

$$V_{nro} = A_L V_{nri} \; . \tag{28}$$

For radar system calculations, it might be beneficial to know the total noise figure of the receiver F_{RXt} which includes the influences of all above-described noise sources:

$$F_{RXt} = \frac{V_{nri}^2}{kT_0 R_0 B_n G_{TL} G_{LNA} G_{MIX} G_{LFF}} \; . \tag{29}$$

Eventually, it is possible to define the total equivalent noise temperature at the receiver T_{eRXt}:

$$T_{eRXt} = (F_{RXt} - 1)T_0 \; . \tag{30}$$

4. Calculated and Measured Values

Based on the above presented formulae, calculations of noise parameters of the realized samples of CW radar sensors were performed. Two types of oscillators (namely DRO and PLL) were tested. The following principal parameters were substituted into the calculations; see Tab. 1. and Tab. 2.

Parameter	Description	Value	Unit
P_{TX}	transmitted power	21.5	dBm
T_0	standard noise temperature	290	K
F_{LNA}	noise figure of RF pre-amplifier	1.8	dB
G_{LNA}	gain of RF pre-amplifier	16.5	dB
G_{MIX}	conversion gain of mixer	-6.5	dB
F_{MIX}	noise figure of mixer	6.5	dB
$B_n = f_{bh}\text{-}f_{bl}$	noise bandwidth, SSB	$19 \cdot 10^3$	Hz
e_n	input noise voltage of LT1028	1.2	nV.Hz$^{-1/2}$
i_n	input noise current of LT1028	1.8	pA.Hz$^{-1/2}$
R_0	load resistance	50	Ω
G_{TL}	transmission line gain	-0.9	dB
R_1	feedback resistor, 1st stage	10	Ω
R_2	feedback resistor, 1st stage	1000	Ω
A_L	voltage gain of LF amplifier	69.4	dB

Tab. 1. Parameters of the tested radar sensors.

Type	f_o	$S_\varphi(f)$
DRO	11.018	$2.5\,10^{-13} + 1/f^2$
PLL	10.750	$2.5\,10^{-11} + 0.5/f^2$
Unit	GHz	1/Hz

Tab. 2. Parameters of the used local oscillators.

It is possible to measure separately the voltages V_{nLA} corresponding to the noise of LF amplifiers, and V_{nLR} comprising the noise of LF amplifiers and noise of RF linear and quasi-linear components:

$$V_{nLR} = \sqrt{V_{nLA}^2 + V_{nRFD}^2} \, . \qquad (31)$$

The latter voltage can be measured by two matched loads replacing the antennas ($G_{AA} = 0$, $P_{ctLF} = 0$, $P_{nPN} = 0$ and $V_{nPN} = 0$). Since V_{nLA} can be easily calculated or measured, from known V_{nLR}, the value of V_{nRFD} can be determined. Unlike that, the measurement of V_{nPN} voltage represents a more difficult problem, for it depends heavily on the value of τ. During the measurement, τ must vary by small increments (i.e. typically 10^1 ps). Since no suitable phase-shifter was available, a new type of the noise measurement based on the employment of a reflecting wall was proposed and verified. In order to change τ by tiny increments, the reflecting metallic wall was placed in front of the radar antennas, while the distance between antennas and the wall was subject to changes, see Fig. 7.
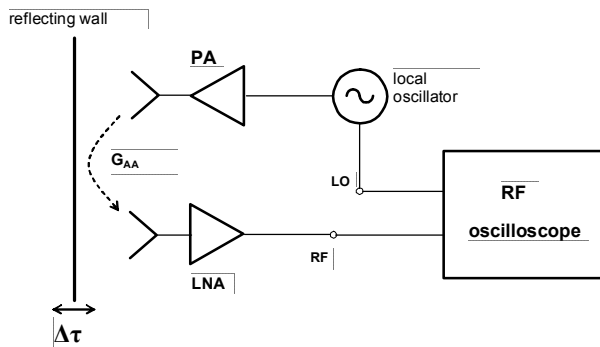

Fig. 7. Variations and measurement of τ.

In each step, time delays τ_1 between the oscillator and an RF input of the mixer, and τ_2 between the oscillator and an LO input of the mixer were measured by the Agilent DCA-J 86100C microwave oscilloscope. The effective values of all noise voltages were measured by the Agilent DSO3202A oscilloscope (via the function 'Measurement' – 'RMS voltage'). A more convenient method based on a computer-controlled variable time-delay circuit is under development. Figs. 8 and 9 show comparisons of the calculated and measured dependences.
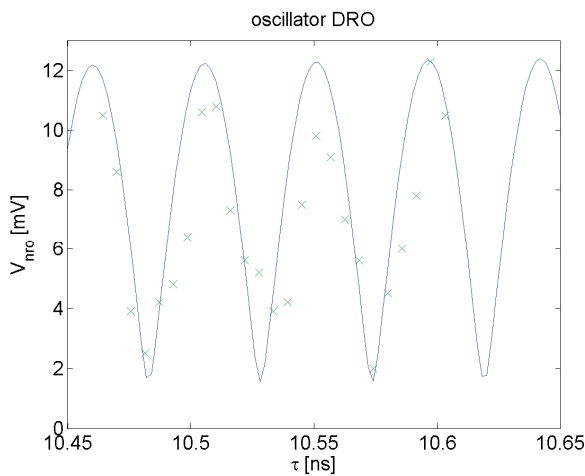

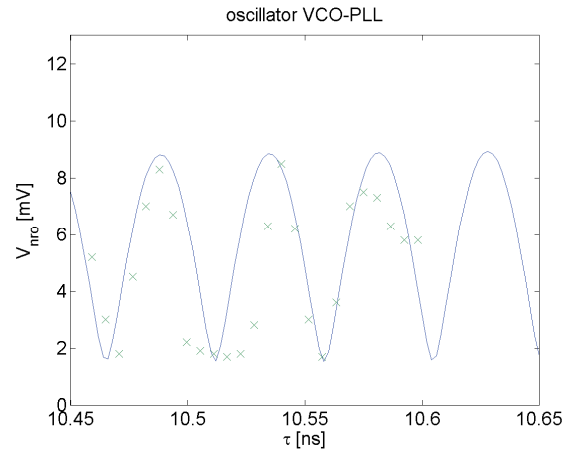**Fig. 8.** Resulting noise voltage as a function of time delay τ, a DRO based sensor.

Fig. 9. Resulting noise voltage as the function of time delay τ, a PLL based sensor.

Both above presented plots show that the measured noise voltages are fairly in accordance with the calculated values. The plots also enable the calculation of other noise parameters and their comparison with the values calculated by the above declared formulae, see Tab. 3. The presented noise parameters are described in detail in Appendix. The values presented in Tab. 3 correspond to the measurement with the reflecting wall, where $G_{AA} = $ -28.5 dB, $\tau = $ 10.5 ns.

Parameter	DRO	DRO	PLL	PLL
	Calculated	Measured	Calculated	Measured
P_{nRFD} [W]	$4.04 \cdot 10^{-15}$	$6.51 \cdot 10^{-15}$	$4.04 \cdot 10^{-15}$	$6.51 \cdot 10^{-15}$
V_{nRF} [V]	$4.50 \cdot 10^{-7}$	$5.71 \cdot 10^{-7}$	$4.50 \cdot 10^{-7}$	$5.71 \cdot 10^{-7}$
P_{nPNmax} [W]	$3.39 \cdot 10^{-13}$	$3.47 \cdot 10^{-13}$	$1.74 \cdot 10^{-13}$	$1.82 \cdot 10^{-13}$
V_{nPNmax} [V]	$4.11 \cdot 10^{-6}$	$4.12 \cdot 10^{-6}$	$2.95 \cdot 10^{-6}$	$2.95 \cdot 10^{-6}$
V_{nLAi} [V]	$2.61 \cdot 10^{-7}$	$2.66 \cdot 10^{-7}$	$2.61 \cdot 10^{-7}$	$2.66 \cdot 10^{-7}$
V_{nrimax} [V]	$4.15 \cdot 10^{-6}$	$4.17 \cdot 10^{-6}$	$2.99 \cdot 10^{-6}$	$3.02 \cdot 10^{-6}$
V_{nromax} [V]	$1.22 \cdot 10^{-2}$	$1.23 \cdot 10^{-2}$	$8.83 \cdot 10^{-3}$	$8.91 \cdot 10^{-3}$
V_{nLR} [V]	$5.20 \cdot 10^{-7}$	$6.29 \cdot 10^{-7}$	$5.20 \cdot 10^{-7}$	$6.29 \cdot 10^{-7}$
$A_L V_{nLR}$ [V]	$1.53 \cdot 10^{-3}$	$1.86 \cdot 10^{-3}$	$1.53 \cdot 10^{-3}$	$1.86 \cdot 10^{-3}$

Tab. 3. Calculated and measured noise parameters – the reflecting wall.

The table shows that in case of relatively high cross-talk (-28.5 dB), the influence of the phase-noise can be very important. The maximum noise voltage V_{nPNmax} caused by the phase-noise is approx. by one order higher than other two components (V_{nRF}, V_{nLAi}).

During the operation of the objective radar sensors, there is no reflecting wall in front of the antennas, so substantially lower G_{AA} values must be considered. In addition, the time-delay τ should be reduced by approx. 1.5 ns. In comparison to the cross-talk created by the reflecting wall, this represents the reduction of time needed for the free space propagation in case of the inherent cross-talk. The calculated and measurable operational noise parameters can be seen in Tab. 4 ($G_{AA} = $ -43 dB, $\tau = $ 9.0 ns). In this table, all noise parameters that include the influence of the specific value phase-noise depending on specific value of τ could not be measured and are not available.

Parameter	DRO	DRO	PLL	PLL
	Calculated	Measured	Calculated	Measured
P_{nRFD} [W]	$4.04 \ 10^{-15}$	$6.51 \ 10^{-15}$	$4.04 \ 10^{-15}$	$6.51 \ 10^{-15}$
V_{nRF} [V]	$4.50 \ 10^{-7}$	$5.71 \ 10^{-7}$	$4.50 \ 10^{-7}$	$5.71 \ 10^{-7}$
P_{nPNmax} [W]	$8.83 \ 10^{-15}$	n.a.	$4.53 \ 10^{-15}$	n.a.
V_{nPNmax} [V]	$6.64 \ 10^{-7}$	n.a.	$4.76 \ 10^{-7}$	n.a.
V_{nLAi} [V]	$2.61 \ 10^{-7}$	$2.66 \ 10^{-7}$	$2.61 \ 10^{-7}$	$2.66 \ 10^{-7}$
V_{nrimax} [V]	$8.44 \ 10^{-7}$	n.a.	$7.05 \ 10^{-7}$	n.a.
V_{nromax} [V]	$2.49 \ 10^{-3}$	n.a.	$2.08 \ 10^{-3}$	n.a.
V_{nLR} [V]	$5.20 \ 10^{-7}$	$6.29 \ 10^{-7}$	$5.20 \ 10^{-7}$	$6.29 \ 10^{-7}$
$A_L V_{nLR}$ [V]	$1.53 \ 10^{-3}$	$1.86 \ 10^{-3}$	$1.53 \ 10^{-3}$	$1.86 \ 10^{-3}$
$T_{eRXtmax}$ [K]	4820	n.a.	3280	n.a.
F_{RXtmax} [dB]	12.5	n.a.	10.9	n.a.

Tab. 4. Calculated and measured noise parameters – the operation.

Based on the fact that all parameters presented in Tab. 3 and Tab. 4 correspond to the noise signals, there is obviously again an acceptable agreement between the calculations and measurements. This fact proves that the presented noise analysis is correct and includes all important noise sources. Beside that, both calculated and measured results indicate a considerable potential influence of the phase-noise on the system noise parameters. The CW radar structures enable the reduction of this influence to zero by ensuring the optimum τ. In practice, the time delay of the cross-talked signal can vary due to external factors, such as rain drops on antenna radoms. Therefore, the optimum phasing has not been applied so far, and the system design was based on maximum values corresponding to (18).

During the operation, the noise voltage at the output of the radar sensor will lie between V_{nromax}, which is an upper limit corresponding to the maximal influence of the phase-noise, and $A_L V_{nLR}$, which corresponds to the zero influence of the phase-noise. Due to a substantially lower cross-talk (-43 dB), the influence of the phase-noise is in this case substantially lower.
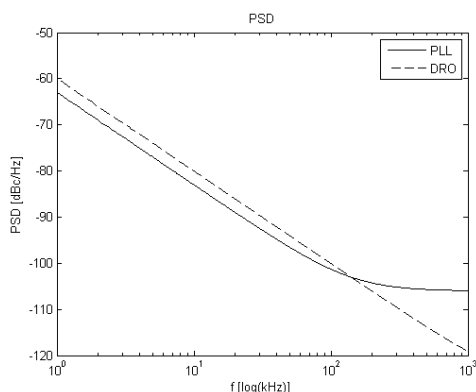

Fig. 10. Approximations of phase noise of DRO and PLL based oscillators as function of frequency off-set f.

Presented results enable also the comparison of the influence of the DRO and PLL based local oscillators, see Tab. 2 and Fig. 10. Although having by 20 dB higher value

of the white phase noise in a high frequency off-set region, the PLL based oscillator shows lower values of the noise PSD in a low frequency off-set region. That is why, for relatively low Doppler frequencies (up to 20 kHz in our case), the employment of the PLL based oscillator results in obviously lower influence of the phase noise (e.g. the P_{nPNmax} values) in comparison with the DRO version. The same phenomenon can be seen when comparing Fig. 8 and Fig. 9. For the higher values of the processed Doppler frequencies (above 140 kHz), the DRO based oscillators can be beneficial.

The AD system based on a slightly modified version of the above described CW radar sensors, was subject to many practical tests, see e. g. the reference [9]. The results show a very good efficiency and reliability of the protection of military vehicles by means of AD even against the most dangerous cumulative missiles. Among the reasons of this positive behavior, favorable noise parameters of the used radar sensors can be ranked.

5. Conclusions

Even relatively simple CW radar sensors can be, in conjunction with other sensors, effectively used in the AD systems. They show no blind-zone and are able to detect even very fast-flying missiles. In order to ensure as high operation reliability as possible, it is necessary to have their noise behavior 'under control'. The derived noise analysis includes RF noise sources, LF noise sources and the contributions of the phase-noise of the local oscillator. The noise analysis was verified on the samples of radar sensors developed for testing the designed AD system.

The performed measurements include a newly developed method of the noise measurement based on the employment of the reflecting wall. The method enables measuring the influences of the time-delay between the reference and cross-talked signals on the resulting output noise voltage. The calculated and measured results show a fairly good agreement. Besides that, they provide a good insight into the noise behavior of the objective sensors and reveal the importance of the phase-noise. Its incidence depends upon the time-delay between the cross-talked and reference signals, and also upon magnitude of the cross-talked signal. In order to reduce this noise source, it is possible to decrease the cross-talk, or to find the optimum time-delay between the cross-talked and reference signals. The developed noise analysis is applicable, with small modifications, even for the design of more complex CW radar structures, e. g. frequency hopping radars or modulated CW radars.

Due to the verification of the noise analysis by means of the measurements with the reflecting wall, it was possible to calculate the operational parameters of the CW radar sensors utilized for testing the developed AD systems. The calculated parameters were used for the development of both the sensors and consequent signal processing.

Appendix

Calculated and measured noise parameters:

Param.	Unit	Description
P_{nRFD}	W	DSB noise power generated by linear and quasi-linear components at R_0 load
V_{nRF}	V	Noise voltage at R_0 load corresponding to P_{nRFD}
P_{nPNmax}	W	Max. value of noise power to R_0 load resulting from local oscillator phase-noise
V_{nPNmax}	V	Max. value of noise voltage at R_0 load resulting from local oscillator phase-noise
V_{nLAi}	V	Noise voltage of LF amplifiers referred to input
V_{nrimax}	V	Resulting noise voltage at R_0 load corresponding to maximum of phase-noise
V_{nromax}	V	Resulting noise voltage at output of radar corresponding to maximum of phase-noise
V_{nLR}	V	Noise voltage at R_0 load corresponding to zero influence of phase-noise
$A_L V_{nLR}$	V	Noise voltage at output of radar corresponding to zero influence of phase-noise
F_{RXtmax}	-	Noise figure comprising all noise sources, corresponds to max. of phase-noise
$T_{eRXtmax}$	K	Equivalent noise temperature comprising all noise sources, corresponds to max. of phase-noise

References

[1] RASSHOFER, R. H., BIEBL, E. M. A direction sensitive, integrated, low cost Doppler radar sensor for automotive applications. *1998 MTT-S International Microwave Symposium Dig.*, 98.2, p. 1055-1058.

[2] ROSELLI, L., ALIMENTI, F., COMEZ, M., PALAZZARI, V., PLACENTINO, F., PORZI, N., SCARPONI, A. A cost driven 24 GHz Doppler radar sensor development for automotive applications. In *35th European Microwave Conference*. Paris (France), 2005, CD, p. 2059-2062.

[3] KIM, J. G., SIM, S. H., CHEON, S., HONG, S. 24 GHz circularly polarized Doppler radar with a single antenna. In *35th European Microwave Conference,* Paris (France), 2005, CD, p. 1383-1386.

[4] KIM, S. G., KIM, H., LEE, Y., KHO, I. S., YOOK, J. G. 5.8 GHz vital signal sensing Doppler radar using isolation-improved brach-line coupler. In *3rd European Radar Conference*, Manchester (UK), 2006, CD, p. 249-252.

[5] DROITCOUR, A. D., BORIC-LUBECKE, O., LUBECKE, V. M., LIN, J., KOVACS, G. T. A Range correlation and I/Q performance benefits in single-chip silicon Doppler radars for noncontact cardiopulmonary monitoring. *IEEE Trans. on MTT*, vol. MTT-52, no. 3, March 2004, p. 838-848.

[6] ISA, M., WU, W. Microwave Doppler radar sensor for solid flow measurements. In *36th European Microwave Conference*, Manchester (UK), 2006, CD, p. 1508-1510.

[7] RANDUS, M., HUDEC, P., HOFFMANN, K. Short-range detection and measurement of small high-speed objects in microwave frequency region. In *Proceedings of the 70th ARFTG Measurement Conference*. Phoenix (Arizona), 2007.

[8] HUDEC, P., RABOCH, J., RANDUS, M., HOFFMANN, K., HOLUB, A., SVANDA, M., POLIVKA, M. Microwave radar sensors for active defense systems. In *Proceedings of the EuRAD Conference*. Rome (Italy), 2009.

[9] HUDEC, P., PLASIL, J., DOHNAL, P. Digital signal processing applied to radar sensors operated in active defense systems. In *Proceedings of the EuRAD Conference*. Paris (France), 2010.

[10] Linear Technology. *LT1028/LT1128 Ultra Low Noise Precision High Speed Op Amps*. [Online] Cited 2011-05-05. Available at http://cds.linear.com/docs/Datasheet/1028fa.pdf.

[11] UNDERHILL, M. J. Fundamentals of oscillator performance. *Electronics & Communication Engineering Journal*, Aug 1992, vol.4, no.4, p. 185-193. Available at: http://ieeexplore.ieee.org/stamp/stamp.jsp?tp=&arnumber=159001&isnumber=4094

[12] ROHDE, U. L., NEWKIRK, D. P. *RF/Microwave Circuit Design for Wireless Applications*. Page 832. Publisher: John Wiley and Sons, 2000,. ISBN:0471298182, 9780471298182.

About Authors ...

Vojtech JENIK was born in Prague in 1985. He received his M.Sc. in Telecommunications and Radio Engineering from the Czech Technical University in Prague in 2010. He is a PhD. student at the Department of Electromagnetic Field. His research interests include microwave sensors for detection of high speed moving objects and other microwave measurement methods.

Premysl HUDEC graduated from the Czech Technical University in Prague in 1982. In the same year, he joined the Department of the Electromagnetic Field, where he is working as an associated professor. His teaching duties include CAD of microwave circuits and microwave measurement. In the recent years, his research activities have been focused on the employment of microwave technology in security applications. It includes the design of different types of microwave radar sensors for active defense systems and development of RFID systems for a long-range identification. He is an author of numerous conference papers, journal articles and patents.

Petr PANEK was born at Rakovnik, Czech Republic in 1957. He received his M.Sc. and Ph.D. degrees in Electrical Engineering at the Czech Technical University in Prague, Czech Republic in 1982 and 1988, respectively. He is with the Institute of Photonics and Electronics, Academy of Sciences of the Czech Republic, Prague. He has a long experience in industrial R&D. His main research interests are time measurement and radio positioning.